

Interparticle Capillary Forces at a Fluid–Fluid Interface with Strong Polymer-Induced Aging

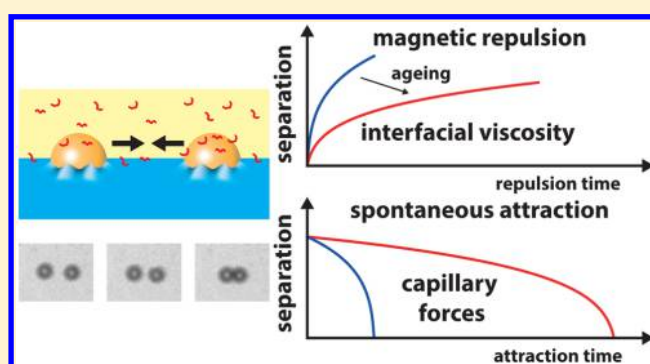
Stefano Cappelli,^{†,‡,Ⓛ} Arthur M. de Jong,^{†,‡} Jean Baudry,[§] and Menno W. J. Prins^{*,†,‡,Ⓛ,Ⓛ}

[†]Department of Applied Physics, [‡]Institute for Complex Molecular Systems (ICMS), and [Ⓛ]Department of Biomedical Engineering, Eindhoven University of Technology, Eindhoven, The Netherlands

[§]Laboratoire Colloïdes et Matériaux Divisés (LCMD), ESPCI Paris, PSL Research University, CNRS UMR8231 Chimie Biologie Innovation, F-75005, Paris, France

Supporting Information

ABSTRACT: We report on a measurement of forces between particles adsorbed at a water–oil interface in the presence of an oil-soluble polymer. The cationic polymer interacts electrostatically with the negatively charged particles, thereby modulating the particle contact angle and the magnitude of capillary attraction between the particles. However, polymer adsorption to the interface also generates an increase in the apparent interfacial viscosity over several orders of magnitude in a time span of a few hours. We have designed an experiment in which repeated motion trajectories are measured on pairs of particles. The experiment gives an independent quantification of the interfacial drag coefficient (10^{-7} – 10^{-4} Ns/m) and of the interparticle capillary forces (0.1–10 pN). We observed that the attractive capillary force depends on the amount of polymer in the oil phase and on the particle pair. However, the attraction appears to be independent of the surface rheology, with changes over a wide range of apparent viscosity values due to aging. Given the direction (attraction), the range ($\sim\mu\text{m}$), and the distance dependence ($\sim 1/S^5$) of the observed interparticle force, we interpret the force as being caused by quadrupolar deformations of the fluid–fluid interface induced by particle surface roughness. The results suggest that capillary forces are equilibrated in the early stages of interface aging and thereafter do not change anymore, even though strong changes in surface rheology still occur. The described experimental approach is powerful for studying dissipative as well as conservative forces of micro- and nanoparticles at fluid–fluid interfaces for systems out of equilibrium.



INTRODUCTION

The strong adsorption of colloidal particles to fluid–fluid interfaces is used and studied for many applications, such as food technology,^{1,2} biomedicine,^{3,4} and materials science.^{5–7} The interface represents a plane where micro- and nanoparticles can laterally diffuse and self-organize into ordered structures,^{8,9} and the properties on macroscopic length scales depend on the materials of particles and fluids, the shape of the particles, and the spatial dimensions between the particles.⁷ The resulting particle assemblies can be deposited on solid substrates for surface patterning⁶ or can be used to modify the rheology of the interface.^{10,11} Furthermore, the use of polyelectrolytes in combination with nanoparticles is becoming an attractive approach for the single-step production of microcapsules, which is relevant for biomedical applications, cosmetics, and food science.^{4,12} These technologies strongly depend on the knowledge and control of interparticle forces, which may change during sample preparation. This calls for the development of new tools, able to measure interparticle interactions at fluid–fluid interfaces with single-particle

resolution and applicable to systems with a strongly time-dependent character.

The interactions of particles at fluid–fluid interfaces differ both in nature and range with respect to the interactions in a single fluid phase. A particle at a polar/nonpolar interface generates an electric dipole that is responsible for long-ranged electrostatic interactions.^{13–15} Deformations of the fluid interface are responsible for long-ranged capillary interactions, driven by surface minimization.^{16–18} The resulting interparticle force depends on how the interface is deformed at the three-phase boundary, e.g., by gravity, shape anisotropy, or surface heterogeneities.^{19–22}

The interparticle potential can be measured with both indirect and direct experimental approaches. When the concentration of colloids at the interface is sufficient to form a 2D crystal (surface fraction $\phi_s \geq 0.2$), Zwanzig et al.²³ demonstrated that the interaction potential can be calculated

Received: October 27, 2016

Revised: December 23, 2016

Published: December 30, 2016

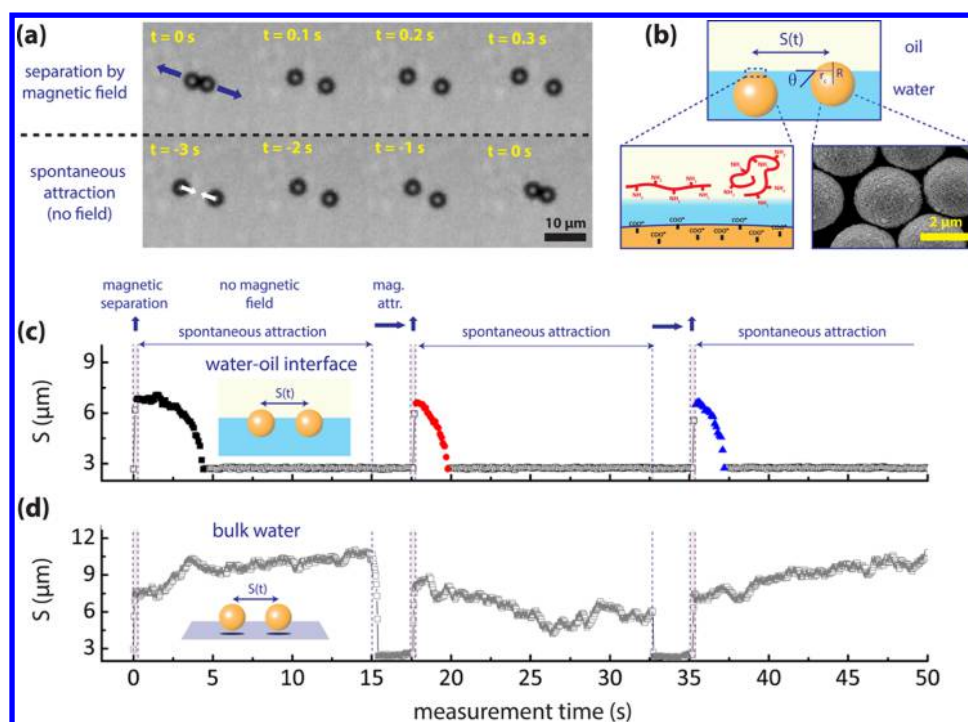


Figure 1. Principle of the colloidal attraction experiment. (a) Pairs of superparamagnetic particles at a water–oil interface are separated by briefly applying a magnetic field in the direction normal to the interface.³⁸ Thereafter, in the absence of a magnetic field, spontaneous attraction is observed. (b) Sketch of magnetic particles at a water–oil interface in the presence of an amino-modified silicone polymer. Particles adsorb to the interface only in the presence of the polymer, as a result of electrostatic interactions between the carboxylated surface of the magnetic particles, with negative charges, and the amine group of the polymer exposed to the water phase, with positive charges.^{4,39} The scanning electron microscopy (SEM) image of M270 particles ($2R = 2.8 \mu\text{m}$) shows a particle surface roughness of about 50 to 150 nm. Panels c and d show time traces of the center-to-center separation distance S during colloidal attraction experiments for particles at a water–oil interface and for particles in bulk water moving on a glass substrate, respectively. (c) Highlighted points (colored solid symbols) show the trajectories of spontaneous (nonmagnetic) particle attraction, which is observed for particles adsorbed to the water–oil interface (as in panel c) but is not observed for particles in bulk water (as in panel d). This proves that the spontaneous attraction is caused by the fluid–fluid interface and not by magnetic forces.

from the dependence of the macroscopic shear modulus on surface coverage. However, this approach is sensitive to both hydrodynamic interactions and defects in the crystal, providing a lower limit for the interaction force.²⁴ At a low surface fraction of colloids at the interface ($\phi_s \rightarrow 0$), it is possible to measure the pair correlation function $g(r)$ from digital images and then determine the pair interaction potential from fitting the Boltzmann distribution $U(r) = -k_B T \ln g(r)$.^{18,24} This method requires a large number of particles and images and provides only an average potential. Alternatives have focused on self-assembly processes of anisotropically shaped particles monitored using video microscopy.^{19,21,25,26}

Direct methods are able to measure interactions on single pairs of particles. The studies have been mainly restricted to optical tweezers experiments.^{27–29} Force versus distance curves were measured on pairs of particles within a force range of 0.1–100 pN and with a position accuracy of a few nanometers, from which the interaction potential is determined. These experiments have shown that electrostatic and capillary forces can be modulated by the addition of salts, surfactants, or polyelectrolytes as a result of changes in particle wettability, particle surface charges, and surface tension.³⁰ On the other hand, the adsorption of macromolecules to the interface is responsible for changes in the interfacial rheology,^{31,32} which may contribute to variations of interparticle interactions over time. Several microrheology techniques are available to monitor the interfacial viscosity, such as magnetic microneedles,^{33,34} magnetic microbuttons,³⁵ and optical tweezers, but only the

latter is suited to measure interparticle forces. Most of the studies have been limited to measurements of capillary forces for interfaces at equilibrium. Time-dependent interparticle interactions at fluid interfaces have been previously reported only for a particle ensemble but are not yet fully understood.^{18,36,37} The study of nonequilibrium systems poses several challenges, as changes in surface rheology and interparticle forces can be very large and can occur over a wide range of time scales.

Here, we propose a method to disentangle conservative capillary forces from dissipative viscous forces. We study attractive capillary forces between spherical magnetic particles adsorbed at a water–oil interface in the presence of an oil-soluble amino-modified silicone polymer. The cationic polymer penetrates to the water side of the interface and interacts electrostatically with the negatively charged particles. This in turn modulates the particle contact angle and the magnitude of capillary attraction between the particles. Moreover, polymer adsorption to the interface generates changes in the surface rheology over several orders of magnitude in a time span of a few hours. We quantify the interfacial drag coefficient of pairs of particles using the intrapair magnetophoresis (IPM) technique, as described in a previous paper.^{38,39} Pairs of magnetic particles are displaced using well-controlled magnetic dipole–dipole forces ($\sim \text{pN}$), allowing one to measure changes in drag coefficients within a few seconds and over large variations (10^{-7} to 10^{-4} N s/m). In the absence of a magnetic field, we record multiple trajectories of particle attraction

utilizing the same particle pair (Figure 1). The experiment gives an independent quantification of the interfacial drag coefficient and of the magnitude of nonviscous interparticle forces in the system.

MATERIALS AND METHODS

Materials. Silicone-based amino-functionalized polymer (KF8004) was provided as samples by Shin-Etsu Silicones Europe B.V. The polymer is soluble in the oil phase but not in water. The oil phase is isononyl-isononanoate (Lanol 99, Seppic, $\eta_{\text{oil}} = 6$ mPa s, and polymer concentrations are prepared by weighting the components. The aqueous phase consists of phosphate-buffered saline (PBS), prepared by dissolving PBS tablets (PBS tablets, pH 7.4, Sigma-Aldrich) in 200 mL of ultrapure water (resistivity > 18.2 M Ω -cm) according to the supplier and then further diluting to a final concentration of 20 mM. All of the components were used as received from the suppliers without any further purification.

Carboxylic superparamagnetic particles (Dynabeads M-270 carboxylic acid, diameter $2R = (2.8 \pm 0.1)$ μm , Life Technologies) were used to quantify the particle interfacial drag coefficient and interparticle interactions. In the presence of a magnetic field, the induced magnetization follows a Langevin function, with a particle-to-particle variation of magnetic susceptibility of about 8%.³⁸ Larger carboxylic ferromagnetic particles (CFM-300-5 carboxylic acid, ferromagnetic, nominal size 28–34.9 μm , Spherotech) were used to study the particle dynamic contact angle at the water–oil interface for different concentrations of amino-polymer (section S5 of the Supporting Information). Both particle types were magnetically washed four times in ultrapure water in order to remove surface-active elements present in the storage buffer and were then dispersed in each corresponding buffer in a ratio of 1:10⁴ from the stock solution. The fluid cell and the setup required to actuate magnetic particles are described elsewhere.³⁹

Quantification of Particle Drag Coefficients and Attractive Capillary Interactions at a Water–Oil Interface. We quantify the particle forces at the water–oil interface with intrapair magnetophoresis (IPM).^{38,39} Pairs of magnetic particles are attracted and repelled by well-controlled magnetic dipole–dipole forces \vec{F}_{magn} induced by an external magnetic field. The magnetic forces are balanced by electrostatic forces \vec{F}_{el} , capillary forces \vec{F}_{cap} , and drag forces \vec{F}_{drag} , with a total force expression of

$$\vec{F}_{\text{magn}} + \vec{F}_{\text{cap}} + \vec{F}_{\text{el}} + \vec{F}_{\text{drag}} = 0 \quad (1)$$

The magnetic repulsion force between two magnetic dipoles with an out-of-plane orientation can be approximated by the relation³⁸

$$F_{\text{magn}} = \frac{3\mu_0 m_{d,1} m_{d,2}}{4\pi S^4} \quad (2)$$

where S is the center-to-center separation distance between the particles, μ_0 is the vacuum permeability, and $m_{d,i}$ is the magnitude of the induced magnetic moment (in units of A m²) of particle i .

Capillary forces originate from the overlap of deformations of the interface around the particles. Danov et al.^{20,40} formally treated the concave and convex deviations of the meniscus shape from planarity as positive and negative capillary charges, by analogy to electrostatics. The interparticle potential can then be described as a superposition of capillary multipoles of order m , where $m = 0, 1, 2, \dots$ represents capillary charges, dipoles, quadrupoles, and so forth. In the far field ($S \gg R_A + R_B$) and for $m_A, m_B \geq 1$, the interaction energy can be approximated as^{16,18}

$$\Delta E_{\text{AB}}(S) \approx -12\pi\gamma H_A H_B \cos(m_A \phi_A + m_B \phi_B) \frac{r_A^{m_A} r_B^{m_B}}{S^{m_A + m_B}} \quad (3)$$

where γ is the surface tension between the two fluid phases, H_i is the undulation amplitude of the menisci around particle i with orientations ϕ_i , and r_i is the radius of the particle cross-section with the interface, which is related to the equilibrium contact angle θ by the geometrical relation $r_c = R \sin \theta$ (Figure 1b). In the near field ($S \approx R_A + R_B$), eq 3 should be expanded because higher-order terms in the interaction

potential become relevant. For particles with a diameter below 10 μm , deformation due to gravity can be neglected (Eötvös number $Eo \ll 1$). In the absence of any external torque, the first nonvanishing term is the quadrupolar interface deformation ($m = 2$), and the resulting force between two identical particles equals the negative of the gradient of the interparticle potential of eq 3, yielding

$$F_{\text{cap}} = -F_{0,\text{cap}} \left(\frac{2R}{S} \right)^5 \quad \text{with } S \geq 2R \quad (4)$$

where $F_{0,\text{cap}} = \frac{3\pi}{2R} \gamma H_2^2 \sin^4 \theta$ is the closest-proximity capillary force, i.e., the force with condition $S = 2R$. In the derivation of eq 4, we neglected the particle rotational degrees of freedom, i.e., $\phi_{A,B}$ in eq 3. Rotations around the axes parallel to the plane of the interface are strongly inhibited by interfacial forces.^{39,41} Rotations around the axis normal to the plane of the interface may occur under rotational Brownian motion and capillary forces. In the capillary attraction experiments in this article, the attraction times vary between a few seconds to several tens of seconds, depending on the magnitude of the particle drag. On this time scale, the particle rotation due to Brownian motion is on the order of tens of degrees, so we can assume that the particle pair dynamically equilibrates to the minimum in the interaction potential.

Electrostatic forces originate from an asymmetric distribution of charges across the interface. The resulting force is always repulsive, it may extend over several micrometers, and it can be modulated by changing the charged species on the particle surface, the particle three-phase contact angle, or the ionic strength of the aqueous subphase.^{13,14,18,20,30} Although a consensus on the underlying physical origin of the electric dipole is still lacking,^{27,42} the electrostatic dipole–dipole force between two particles at a fluid–fluid interface can be described by the functional form¹⁸

$$F_{\text{el}} = F_{0,\text{el}} \left(\frac{R_A + R_B}{S} \right)^4 \quad (5)$$

where $F_{0,\text{el}}$ is the closest-proximity force, i.e., for $S = R_A + R_B$, that depends on the particles and fluid properties and R_i is the radius of particle i .

The hydrodynamic force acting on a particle moving in a Newtonian fluid is proportional to the particle velocity, with a particle drag coefficient f that depends on the particle size and fluid viscosity. For a particle moving in a fluid–fluid interface, the particle drag coefficient depends on the viscosity ratio between the two phases, on the three-phase contact angle, and on the interfacial viscosity η_s . The relation between f and η_s relies on the assumptions of the underlying hydrodynamic models,^{32,43–45} and depends on the actuation dynamics of the probe (e.g., rotation or translation).⁴⁶ In a previous paper,³⁹ we addressed these issues related to the IPM measurement technique and we demonstrated that the response of the interface for the material system used in this study is essentially viscous. Here, we will characterize the aging of the interface through the particle drag coefficient f .

In absence of a magnetic force ($\vec{F}_{\text{magn}} = 0$), the particle motion is determined by electrostatic, capillary and drag forces. We performed experiments in absence of a magnetic force using different ionic strengths of the aqueous phase. For an aqueous solution containing 150 mM PBS, no significant repulsion or attraction was measured for all polymer concentrations (data not shown), while experiments with an aqueous solution with 20 mM PBS showed significant attractive forces. The contribution of the dissociated charges on the water side of the interface is negligible for both PBS concentrations, with Debye lengths of $\kappa^{-1} \approx 0.8$ and 2 nm for 150 and 20 mM PBS, respectively. A small number of surface charges may be present in the oil phase due to residual water in the nonpolar solution or to water trapped in cavities present on the surface of rough particles. This could be sufficient to generate long-ranged repulsive forces.²⁷ However, in our experiment the negative charges exposed to the oil side of the interface are expected to be counterbalanced by the positive charges of the cationic polymer.⁴⁷ Indeed, in the experiments no distance dependence of $\sim 1/$

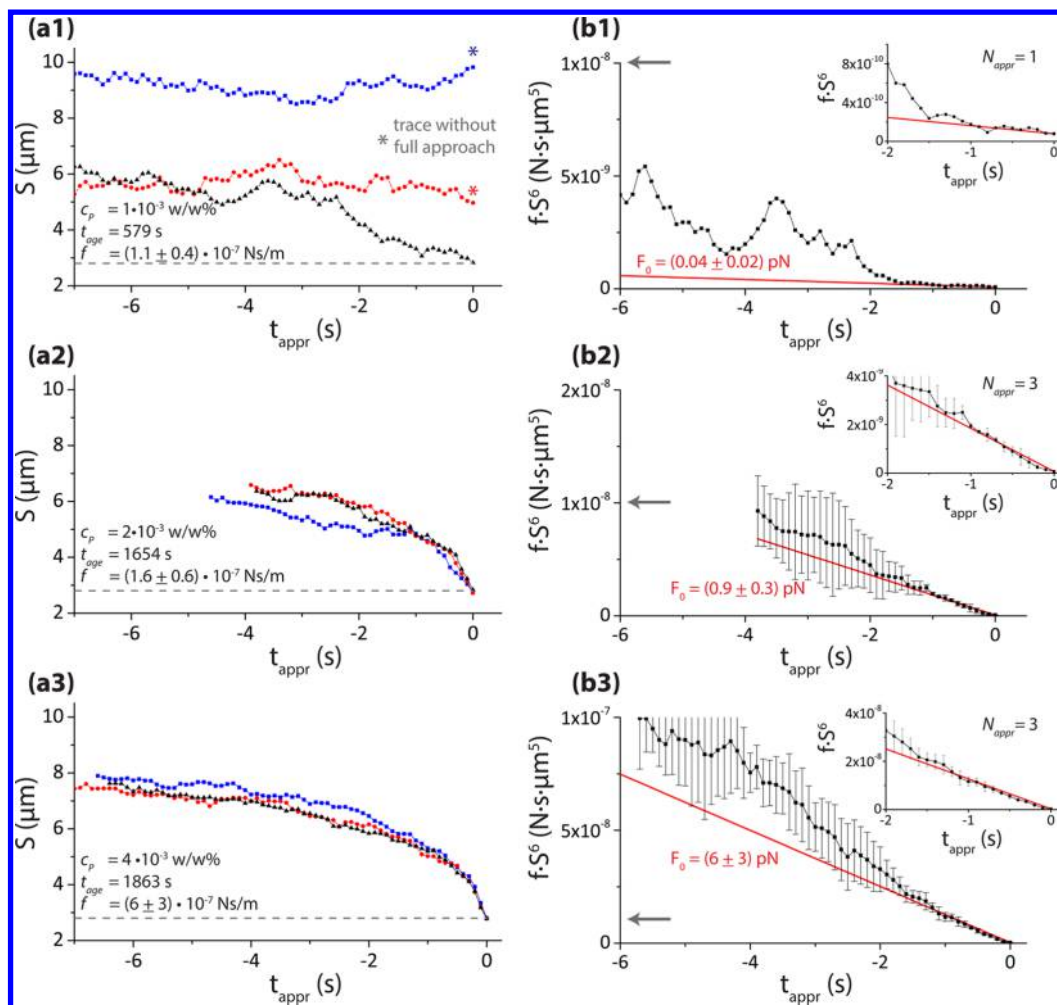


Figure 2. Colloidal attraction experiments for particles at the water–oil interface for increasing concentrations of polymer in the oil phase (c_p) and different aging times (t_{age}). (a) Center-to-center separation S as a function of particle approach time t_{appr} . The dashed line represents $S = 2R = 2.8 \mu\text{m}$. Each individual panel (a1, a2, and a3) shows three approach trajectories measured on the same particle pair. Different panels (a1, a2, and a3) show different particle pairs. (b) To quantitatively compare measurements performed at different aging times (i.e., to take into account the drag coefficient f of particles (as described in section S4) experienced at a different t_{age}), we plot attraction curves expressing fS^6 as a function of particle approach time for particles with full approach in panel a (i.e., $S = 2R$ at $t_{\text{appr}} = 0$). Points and error bars in panels b2 and b3 represent the mean and the standard deviation. The solid red line is a fit according to eq 7, performed only on the linear part of fS^6 attraction curves close to $t_{\text{appr}} = 0$, as shown in the insets. From the fit, we extract the value of the capillary force $F_{0,\text{cap}}$ (i.e., the capillary force at $S = 2R$). For comparison, the gray arrow on the y axis indicates equal magnitude in the different panels.

S^4 was observed. Therefore, we conclude that electrostatic forces can be neglected in the experiments. Using eq 1, with $\vec{F}_{\text{el}} = 0$ and $\vec{F}_{\text{drag}} = \frac{f}{2} \frac{dS}{dt}$, eqs 2 and 4, the equation of motion is

$$\frac{f}{2} \frac{dS}{dt} = F_{0,\text{magn}} \left(\frac{2R}{S} \right)^4 - F_{0,\text{cap}} \left(\frac{2R}{S} \right)^5 \quad (6)$$

where we introduced the closest-proximity magnetic force $F_{0,\text{magn}} = \frac{3\mu_0 m_d,1 m_d,2}{4\pi(2R)^4}$ by analogy to the notation we used for the expression of the capillary force; see section S3 in the Supporting Information for details on the derivation. The left side of eq 6 represents the dissipative drag force. The right side of eq 6 represents the conservative interparticle magnetic and capillary forces.

To disentangle the conservative interparticle forces from dissipative effects caused by interfacial aging, both $F_{0,\text{cap}}$ and f need to be quantified in eq 6. We designed an experiment in which for every particle pair, repulsion trajectories are measured in the presence of an out-of-plane magnetic field and attraction curves are measured in the absence of a magnetic field. Repulsion trajectories are measured by applying a repulsive field for 4 s, thereby separating the particles by a few particle diameters. Attraction trajectories are measured as follows.

After magnetically positioning the particle pair at $S = 2R$, we use a short repulsive field to separate pairs of magnetic particles. Then, in the absence of any magnetic field, we record motion trajectories of the resulting interaction (Figure 1c) and compute the average of the curves that show the full approach. The procedure is repeated three times (Figure 1c), and the entire motion trajectory can be recorded in about 60 s. During colloidal attraction, magnetic forces are not present (i.e., $\vec{F}_{\text{magn}} = 0$ in eq 1), and the resulting equation of motion can be expressed as

$$S^6 = -\frac{12(2R)^5 F_{0,\text{cap}}}{f} (t - t_0) + S_0^6 \quad (7)$$

With these two measurements, we are able to independently quantify f and $F_{0,\text{cap}}$ using eqs 6 and 7, as our technique provides magnetic forces within a range similar to that of the attractive forces measured in the experiments (in the range of hundreds of fN to tens of pN). Equation 7 is based on eq 3, which is, strictly speaking, valid only in the far field. However, in our experiments we found that eq 7 closely fits the data so that higher multipole orders can be neglected. The analysis method is described in more detail in section S4 of the Supporting Information.

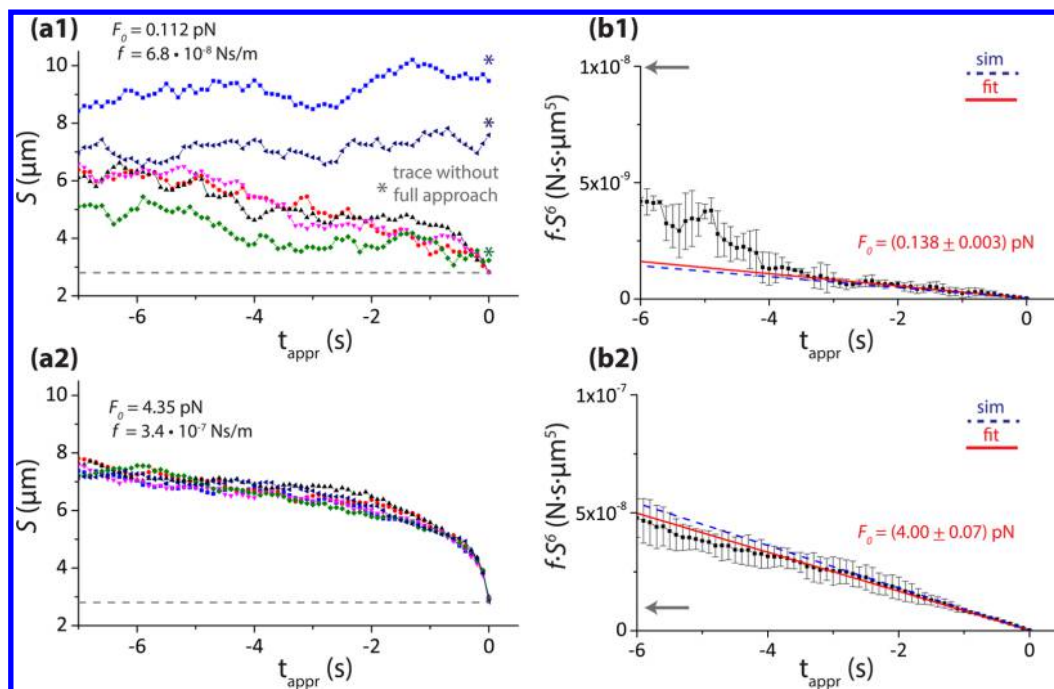


Figure 3. Brownian dynamics simulations for a pair of particles ($R = 1.4 \mu\text{m}$) in the presence of an attractive force as described in eq 4. (a) Center-to-center separation S as a function of particle approach time obtained from six simulations performed with the same set of initial conditions (as indicated in each graph). The dashed line represents $S = 2R = 2.8 \mu\text{m}$. (b) Attraction curves expressing fS^6 as a function of particle approach time. Points and error bars represent the mean and the standard deviation of the curves that show full approach in the corresponding panel (a), i.e., $S = 2R$ at $t_{\text{appr}} = 0$. The solid red line is a fit according to eq 7 of only the initial linear part of the fS^6 attraction curves. The dashed blue line represents the simulated attraction curve without Brownian motion. For comparison, the gray arrow on the y axis indicates equal magnitude in the different panels.

Numerical Methods. We performed Brownian dynamics (BD) simulations in order to generate trajectories of particles that undergo Brownian motion in the presence of a total (conservative) force \mathbf{F} . The aim of BD simulations was twofold. On one hand, we determined the interplay between dissipative (viscous) forces and conservative (capillary) forces. On the other hand, we validated and determined the accuracy of the analysis method as described in the previous section to determine both f and $F_{0,\text{cap}}$. Simulations were performed by following the approach described by Grassia et al.⁴⁸ A massless particle i is moving with a tensor coefficient of linear friction ξ_{ij} and diffusivity tensor $D_{ij} = k_B T / \xi_{ij}$, where $k_B T$ is the Boltzmann energy. The trajectories of particles are obtained by adding at each time step δt a random displacement $\mathbf{x}_i^{\text{ran}}$ to the systematic displacement $\mathbf{F}_i(\xi_{ij}^{-1})\delta t$. If we consider a constant linear friction coefficient $\xi_{ij} = f$ and neglect hydrodynamic interactions between the particles, then BD trajectories $\mathbf{x}_i(t)$ are computed from the relation

$$\mathbf{x}_i^{n+1} = \mathbf{x}_i^n + \frac{\mathbf{F}}{f}\delta t + (2D\delta t)^{1/2}\mathbf{r}_i^n \quad (8)$$

where \mathbf{r}_i^n is a random vector with independent components, each extracted from a uniform distribution over the interval $[-0.5, 0.5]$. The generated random displacements will converge to a Gaussian distribution, provided that a sufficiently small time step and the correct moments of the distribution are taken⁴⁹ (i.e., zero mean and a variance that follows from the dissipation–fluctuation theorem⁵⁰). Simulations were performed with a time step of $\delta t = 2 \times 10^{-5}$ s. We validated this numerical method following the approach proposed by Northrup et al.,⁵¹ as shown in section S1.

RESULTS AND DISCUSSION

We studied the interaction of carboxylic magnetic microparticles at a water–oil interface in the presence of an amino-modified silicone polymer in the oil phase. For an aqueous solution containing 20 mM phosphate-buffered saline (PBS), we observed an attractive interaction between particles over

tens of micrometers, depending on the polymer concentration. On the other hand, polymers are known to adsorb to fluid–fluid interfaces, where interactions between the adsorbed polymers (e.g., hydrogen bonding and hydrophobic or electrostatic interactions) can contribute to large variations of the interfacial shear viscoelasticity^{31,52} on a time scale varying from a few seconds to several hours. We have designed an experiment in which pairs of particles are magnetically separated by a few micrometers using the IPM method. Then, repeated motion trajectories are recorded on the same particle pair. These two independent measurements allow us to disentangle and quantify conservative forces and dissipative effects.

In the next section, we present the results as follows. We first provide examples of colloidal attraction experiments for particles at a water–oil interface for different concentrations of polymer in the oil phase. Then, we use Brownian dynamics simulations to interpret the experiments and to validate our analysis method to quantify capillary and viscous forces. Finally, we quantify the interfacial drag coefficient of particles and attractive capillary forces as a function of polymer concentration, and we discuss the origin of particle attraction and how changes in interfacial viscosity correlate with the conservative attractive capillary force.

Measurements of Colloidal Attractive Interactions. In a typical experiment on particle attraction, pairs of magnetic particles were first separated by a few particle diameters by quickly applying an out-of-plane magnetic field, and then after the field was removed, the field-free motion trajectories were recorded (Figure 1a). To exclude the influence of any magnetic component (e.g., setup, particle magnetic moment) on particle attraction, we performed the same experiment using particles in

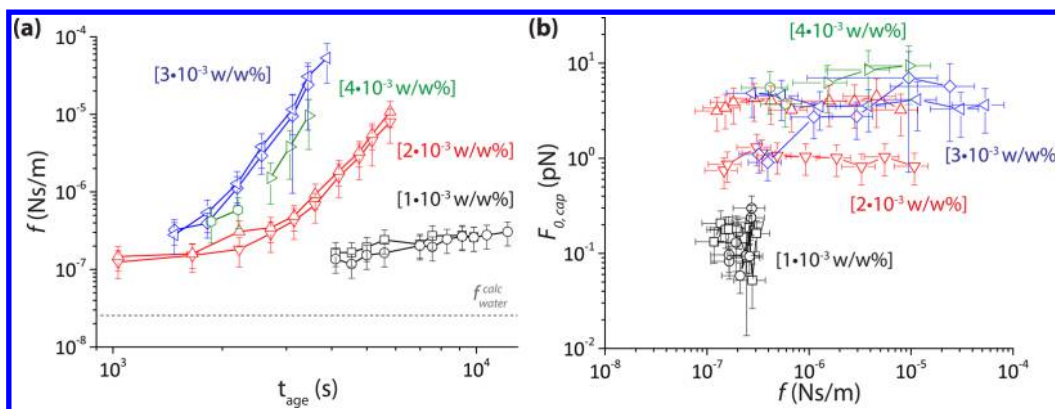


Figure 4. Capillary attraction in the presence of polymer-induced interfacial aging. (a) Interfacial drag coefficient f as a function of interfacial aging time, as measured by IPM experiments.³⁸ Experiments were performed for different initial polymer concentrations c_p (colors) using an aqueous solution with 20 mM PBS. In both graphs, connected symbols represent data recorded for the same particle pair (a total of eight pairs are shown). (b) $F_{0,\text{cap}}$ as a function of f . Error bars include a variation of the particle magnetic moment of 8%³⁸ and the error from the iterative fitting used to estimate the particle drag coefficient f and the capillary attraction force $F_{0,\text{cap}}$, as described in section S4.

bulk water moving on a glass substrate (Figure 1d). In the absence of the magnetic field, the particles showed diffusion with a coefficient of $\sim 0.18 \mu\text{m}^2/\text{s}$, consistent with the diffusion of a sphere with radius $R = 1.4 \mu\text{m}$ in a fluid of viscosity $\eta = 1 \text{ mPa s}$ (free diffusion $D = 0.15 \mu\text{m}^2/\text{s}$) in close proximity to a solid substrate.⁵³ In the absence of a magnetic field, particles did not show a deterministic approach, and attraction was observed only when an in-plane magnetic field was applied.

In Figure 2, we show the results of colloidal attraction experiments for particles at a water–oil interface at increasing initial concentrations of polymer in the oil phase. Panels a1–a3 show the center-to-center separation S as a function of the particle approach time $t_{\text{appr}} = t - t^*$, where t^* is the time for the particle pair to reach $S = 2R$. In each graph, trajectories are recorded on the same particle pair. For $c_p = 1 \times 10^{-3} \text{ w/w\%}$ (a1), the trajectories show either partial or full approach and thermal (Brownian) noise is large as compared to the attractive interaction. Attraction is clearly seen for $S < 4 \mu\text{m}$. For c_p equal to 2×10^{-3} and $4 \times 10^{-3} \text{ w/w\%}$ (panels a2 and a3, respectively), attraction is clearly seen for $S < 6$ and $8 \mu\text{m}$, respectively. The reproducibility of the trajectories is high, with mean standard deviations of 6 and 3%, respectively.

According to the model described by eq 7, the time scale for particle attraction is determined by the initial separation S_0 between the particles, the interfacial drag coefficient of particles f , and the magnitude of the capillary force $F_{0,\text{cap}}$. To take into account the drag coefficient f experienced by the particle at different aging times t_{age} of the interface, we plot the mean and standard deviation of the trajectories that show full approach (denoted as N_{appr}) as the product fS^6 and as a function of the particle approach time t_{appr} (Figure 2b). The drag coefficient f was measured as described in section S4 and later in this section. The data show two distinct regions. For separation distances of a few particle diameters (i.e., for $t_{\text{appr}} < -2 \text{ s}$), the curves show large variations. When the interparticle distance decreases (i.e., for $t_{\text{appr}} > -2 \text{ s}$), the curves approach the relationship described by eq 7 (Figure 2b, insets). The observed increase in the steepness of fS^6 curves points to an increase in the attractive force as a function of polymer concentration.

Brownian Dynamics Simulations of Capillary Attraction. To interpret the attraction curves measured in our experiments and to determine the interplay between attractive forces and thermal fluctuations, we performed BD simulations

using eq 8 to generate trajectories of pair of particles in the presence of an attractive quadrupole force as described by eq 4. In these simulations, we consider the diffusion of particles in a purely viscous fluid with a constant drag coefficient f , and we do not take into account the hydrodynamic interactions between the particles or the relative angular orientation (cf. eq 3), as discussed in the Materials and Methods section.

In each graph of Figure 3a, we show six trajectories of particle attraction obtained with the same set of initial conditions. For a capillary force of $F_{0,\text{cap}}^{\text{sim}} = 0.112 \text{ pN}$ (a1), trajectories show both partial and full approaches, with a high variation between repeated simulations. For increasing values of $F_{0,\text{cap}}^{\text{sim}}$, the range of the attraction extends toward larger interparticle distances S and the encounter rate of particles increases (section S2), with a reduced variation between the trajectories.

Figure 3b shows curves expressing fS^6 as a function of particle approach time. These results show similar features as compared to the experimental trajectories shown in Figure 2b. For a low interacting force (b1) and separations larger than ~ 2 particle diameters, the motion is dominated by thermal fluctuations, as the attractive interacting energy is less than $\sim 2k_B T$. At shorter separations, the attractive interaction overcomes the thermal fluctuations and the curve approaches the expected result based on eq 7. This becomes clearer for increasing values of $F_{0,\text{cap}}^{\text{sim}}$ (b2), where the linear relationship extends toward larger separation distances ($S \simeq 7 \mu\text{m}$). Therefore, to correctly estimate $F_{0,\text{cap}}$ we select the points close to $t_{\text{appr}} = 0$ that follow eq 7. With this approach, we are able to retrieve values of the simulated parameters with an accuracy of 15% or better for $F_{0,\text{cap}}^{\text{sim}} \leq 1 \text{ pN}$ (section S2, Table S2).

The last step required to quantify the capillary force $F_{0,\text{cap}}$ from the experiments shown in Figure 2b is to determine the drag coefficient f of particles at the water–oil interface.

Quantification of the Particle Drag Coefficient f in the Presence of Polymer-Induced Aging. We quantified the drag coefficient f of particles at the water–oil interface from magnetic repulsion experiments using the IPM method.^{38,39} In particular, we studied the aging of the interface by quantifying f as a function of polymer adsorption time for different initial polymer concentrations c_p in the oil phase. We consider the moment at which the interface is formed within the fluid cell as the reference time for the experiments.

For all polymer concentrations, data show an increase in f as a function of the polymer adsorption time (Figure 4a). The time onset for drag increase shifts toward lower adsorption times for higher values of c_p , consistent with a higher diffusive flux of polymer toward the interface. Values obtained from different particle pairs show a variation within the experimental error ($\sim 10\%$), suggesting a homogeneous aging of the interface. As we will show in the next section, capillary forces may become comparable to the magnetic forces used to separate particles. This can be taken into account in our analysis, as described in Materials and Methods and demonstrated with BD simulations (sections S3 and S4).

Quantification of the Colloidal Attractive Force. With the same particle pairs used to quantify f in Figure 4a (represented by open symbols connected by a solid line), we computed the magnitude of the capillary attractive force $F_{0,\text{cap}}$, thus providing a direct correlation between f and $F_{0,\text{cap}}$. Figure 4b shows values of $F_{0,\text{cap}}$ as a function of f for different initial concentrations of polymer in the oil phase (represented as different colors). For a fixed polymer concentration, the capillary attraction varies strongly between different particle pairs, but for a given particle pair, interestingly the capillary attraction does not depend on f or on the amount of polymer adsorbed to the interface. In particular, for $c_p = 2 \times 10^{-3}$ w/w% the represented pairs (up and down red triangles) show similar values for f , but $F_{0,\text{cap}}$ differs by almost 1 order of magnitude. For increasing amounts of c_p , $F_{0,\text{cap}}$ increases with values ranging between ~ 0.1 and ~ 10 pN. For $c_p > 4 \times 10^{-3}$ w/w% (data not shown), the attractive force exceeds the maximum magnetic repulsive force achievable with the configuration of the electromagnets used for this study ($F_{\text{magn}} \simeq 20$ pN) so that particles could not be separated with magnetic forces.

Interpretation of Capillary Attraction Curves. Deformations of fluid–fluid interfaces are known to be responsible for long-range capillary forces and torques between particles. The interparticle potential can be described in terms of capillary multipoles, as described by eq 3, of which the terms depend on the nature of the deformations (e.g., gravity, shape, or chemical anisotropy).^{15,17,19,21,54,55}

Stamou et al. suggested that quadrupolar interface deformations may originate from the pinning of the three-phase contact line to local heterogeneities (e.g., chemical or topological) of the surface of the particles,¹⁶ with the corresponding interacting force as described by eq 4. For the system in this study ($2R = 2.8 \mu\text{m}$, $\gamma = 20$ mN/m, $\rho_p = 1.8$ g/cm³), the Eötvös number is $Eu \simeq 10^{-6} \ll 1$, so deformations due to gravity ($m = 0$) are negligible. For spherical particles, dipolar deformations ($m = 1$) occur in the presence of an external torque or in the presence of surface chemical anisotropy, such as for Janus particles.⁴¹ Superparamagnetic particles are known to have a small remanent magnetic moment. In a previous paper, we demonstrated that the torque required to deform a fluid–fluid interface is well above the maximum available magnetic torque in our system.³⁹ Therefore, the first nonvanishing term in eq 3 is the capillary quadrupole ($m = 2$). The particles used in this study (M270, carboxylic, $2R = 2.8 \mu\text{m}$) have a surface roughness of between 50 and 150 nm, as determined from SEM images (Figure 1b). According to eq 4, a contact angle of $\theta \simeq 16^\circ$ (with $H_2 = 50$ nm, $\gamma = 20$ mN/m) would be sufficient to generate attractive forces as large as $F_{0,\text{cap}} \simeq 1$ pN (Table S1).

The results in Figure 2 show that at large separations, motion trajectories are dominated by thermal (Brownian) motion.

Therefore, we performed BD simulations in order to disentangle the contribution of thermal noise from that due to the attractive force and to validate the analysis method described in section S4. We demonstrated that from the linear part of fS^6 curves (Figure 3b) it is possible to compute the magnitude of the capillary coefficient $F_{0,\text{cap}}$ with an accuracy of 15% or better depending on the magnitude of the attractive force, using the particle drag coefficient f as a fixed parameter (section S2, Table S2). We tested the ability of our approach to discriminate between different orders of attraction by performing BD simulations using $m = m_A + m_B = 3, 4, 5$ in eq 3. With this analysis method, we were able to discriminate between the different orders in the presence of capillary forces greater than a few pN (section S2). The attractive force observed in experiments performed at the water–oil interface (Figure 2) agrees in range ($\sim 10 \mu\text{m}$) and magnitude (\sim pN) with BD simulations (Figure 3). In particular, for increasing concentrations of the amino-polymer in the oil phase, the data clearly reveal an interparticle distance dependence of $\sim 1/S^5$. Although the model describing the interaction potential is valid in the far-field (eq 3), in our data we did not observe significant deviations from eq 4, so higher-order multipoles are not important. Therefore, we interpret the force as being caused by quadrupolar deformations of the fluid–fluid interface induced by particle surface roughness. A similar conclusion was reported by Park et al. from measurements of attractive forces between polystyrene beads confined at a water–decane interface using time-shared optical traps.²⁹ The authors measured forces with the same functional form as eq 4 and magnitudes similar to those shown in Figure 4b, with values that depended on the fluid composition and particle contact angle.

Electrostatic interactions may also occur between particles at fluid–fluid interfaces.¹⁸ The asymmetry of the charge distribution across the interface is responsible for long-ranged repulsive forces that scale with interparticle distance as $\sim 1/S^4$ (cf. eq 5). In our experiments, the negative charges on the particle surface exposed to the oil side of the interface are expected to be counterbalanced by the positive charges of the cationic polymer. Indeed, we did not observe any significant repulsion between the particles nor a distance dependence of $\sim 1/S^4$, so electrostatic interactions can be neglected in our analysis. Other forces, such as van der Waals and solvation forces, may be present but are relevant only at very small distances (\sim nm), with a contribution to the total potential energy of only a few $k_B T$.¹³

Capillary Attraction as a Function of Interface Aging.

We quantified the dissipative effects caused by interfacial aging using the IPM method.^{38,39} With this technique, we were able to quantify the drag coefficient f of particles at the water–oil interface within a few seconds (~ 5 s) and over long time scales (several hours), with a sensitivity to changes in interfacial viscosity as low as $\eta_s = 7 \times 10^{-9}$ N s/m.³⁹ Using BD simulations, we demonstrated that attractive capillary forces can be extracted by the analysis and that the input parameters are retrieved with an accuracy of better than 4% (section S3). When both f and $F_{0,\text{cap}}$ are unknown, our analysis method provided results with accuracies of 9 and 30%, respectively, with respect to the input parameters (section S4, Table S2).

When the interface is formed, polymers adsorb to a pristine interface without steric hindrance. In the absence of an energy barrier for adsorption, at short times ($t \rightarrow 0$) the surface coverage can be estimated by diffusive transport.⁵⁶ For longer times, the adsorption rate is lowered by the limited presence of

remaining unoccupied adsorption sites in the interface.⁵⁷ In the experiments in this article, the interactions between the adsorbed polymers contribute to strong interface aging, as shown by the increase in the particle drag coefficient f over several orders of magnitude ($f \approx 10^{-7}$ to 10^{-4} N s/m, Figure 4a). In a previous paper, we demonstrated that the response of the interface to the motion of the particles is essentially viscous.³⁹

The polymer at the interface is also responsible for the modulation of the position of the particle at the interface (i.e., its contact angle) as a result of electrostatic interactions between the cationic polymer and the carboxyl-functionalized particle (Figure 1).^{4,39} Particles adsorb to the interface only in the presence of the polymer, and for a sufficiently high polymer concentration, the particles transit into the oil phase. Typically, the adsorption of particles to fluid–fluid interfaces is driven by strong interfacial forces, with time scales varying from milliseconds to several minutes or hours.^{58–60} In Figure 4b, we observe that capillary attractive forces increase for increasing polymer concentrations in the oil phase. According to eq 4, $F_{0,\text{cap}}$ depends on the surface tension, the particle contact angle and the interface profile around the particle. Pendant drop surface tension measurements (data not shown) show variations from 30 to 20 mN/m within the same range of concentrations and time scales as the experiments shown in Figure 4, thus contributing to variations of $F_{0,\text{cap}}$ by about 30%. Measurements of the contact angle of larger particles ($2R \approx 34 \mu\text{m}$, with a surface chemical functionality similar to that of small particles, see section S5) showed an increase in the particle contact angle for increasing polymer concentrations, with a time-dependent increase for $c_p > 5 \times 10^{-2}$ w/w% on the time scale of minutes (Figure S7). Therefore, we conclude that attractive capillary forces are dominated by changes in the particle three-phase contact angle rather than the fluid–fluid interfacial tension. This is in agreement with the observation of attractive forces exceeding magnetic repulsive forces for higher concentrations of polymer.

Interestingly, for a fixed polymer concentration, $F_{0,\text{cap}}$ is not correlated with f and differences are dominated by particle-to-particle variation. The data in Figure 4b show that $F_{0,\text{cap}}$ depends only on the initial amount of polymer in the oil phase and does not depend on time (in contrast to f). For low and constant values of f , the density of the polymer at the interface is low ($\eta_s \approx 0$) and the motion of the probe is subphase-dominated (Boussinesq $Bo \ll 1$).⁴⁴ In this regime, the drag of the particle is sensitive to changes in θ . For $c_p = 1 \times 10^{-3}$ w/w%, f increases by a factor of 2, but $F_{0,\text{cap}}$ does not show any correlation with f . Therefore, we attribute the increase in drag to an increase in polymer concentration at the interface, while the contact angle remains constant. For increasing values of f , the motion of the probe is dominated by changes in surface rheology, so measurements of drag are insensitive to changes in the particle contact angle.

The lack of correlation observed between f and $F_{0,\text{cap}}$ suggests that the contact angle of the particles at the interface is fixed in the early stages of polymer adsorption. In our experiments, the polymer exposes the amine groups to the water side of the interface, where they interact with the carboxylic groups on the particle surface. The density of polymer at the interface in the early stages of polymer adsorption ($t_{\text{age}} \approx 0$) is determined by the initial concentration of polymer in the oil phase and on the ionic strength of the aqueous subphase.³⁹ Thereafter ($t_{\text{age}} > 0$), the further accumulation of polymers at the water–oil interface

contributes to an increase in the interfacial viscosity, apparently without changing the capillary forces between the particles. The variation of capillary force between particle pairs observed in Figure 4b may be caused by differences in the particle surface structure at the contact line, in the particle contact angle, and in the polymer adsorption properties. Further research is needed to disentangle these mechanisms and further clarify the origins of polymer-mediated particle adsorption in relation to contact line motion and interface aging.

CONCLUSIONS

We have used magnetic particles to investigate interparticle capillary forces at a water–oil interface with strong polymer-induced aging. The colloidal attraction experiments give an independent quantification and a direct correlation of the interfacial drag coefficient (10^{-7} – 10^{-4} Ns/m) and the nonviscous interparticle capillary forces (0.1–10 pN) in the system. We have validated the method by performing Brownian dynamics (BD) simulations, showing good qualitative and quantitative agreement with experiments. Given the direction (attraction), the range ($\sim \mu\text{m}$), and the distance dependence ($\sim 1/S^5$) of the observed interparticle force, we interpret the force as being caused by quadrupolar deformations of the fluid–fluid interface induced by particle surface roughness, a mechanism proposed by Stamou et al.¹⁶

The magnitude of the attractive force was modulated by the addition of a cationic polymer in the oil phase, where the amine groups of the polymer exposed to the water phase (with positive charges) interact electrostatically with the carboxylic groups (with negative charges) on the surface of the particles.⁴ The increase in the attractive force for increasing concentrations of polymer in the oil phase are consistent with an increase in the particle three-phase contact angle (i.e., the particle cross-section with the interface (cf. eq 3)), as confirmed by contact angle measurements (S5). Surprisingly, for a fixed polymer concentration in solution, the magnitude of the attractive capillary force shows no dependence on time, even though the viscous forces change over several orders of magnitude. These results show that the dissipative effects of interfacial viscosity stabilize much more slowly than the conservative capillary forces between particles at the fluid–fluid interface. The different time scales could be related to different dependencies on interfacial polymer density. The interfacial viscosity may depend much more nonlinearly on the interfacial polymer density than the particle contact angle does because of nonlinear mechanisms such as polymer conformational changes and polymer entanglement.^{61,62} Ideally, one would like to know the time dependence of the interfacial polymer density at the fluid–fluid interface as well as at the fluid–particle interface. In follow-up research, it will be interesting to test such hypotheses on the dissipative versus conservative interfacial forces, with theoretical studies as well as experiments.

To our knowledge, this represents the first study of interparticle capillary forces in a fluid–fluid system far from equilibrium, which gives new opportunities. A current issue in particle-based microrheology is that for a low Boussinesq number the interfacial drag coefficient of particles is sensitive to changes in the particle contact angle.^{32,46} Measured variations in the capillary attraction, together with surface tension measurements (e.g., with a Langmuir trough) could be used to indirectly determine changes in the particle contact angle, thereby helping to obtain more reliable rheological parameters.

The availability of magnetic colloids with a tailored surface roughness would allow one to further investigate the relation between attractive capillary forces and surface structures. In particular, IPM could be used to study capillary interactions at different length scales. In the far field ($S \gg 2R$), capillary interactions can be described as a superposition of capillary multipoles, with the quadrupolar term being the leading one.^{16,20,21} In the near-field ($S \approx 2R$), the interaction is dominated by the shape details of the undulated meniscus around the particle, and higher orders may appear. Moreover, rotational dynamics could be studied by applying an in-plane rotating magnetic field.⁶³ These experiments could be compared with lattice Boltzmann simulations,⁶⁴ where the interaction potential is derived directly from the shape of the interface around the particles. We foresee that IPM will help scientists to shed light on the complex interaction of micro- and nanoparticles at fluid–fluid interfaces for a wide range of materials, with particular interest for systems out of equilibrium.

■ ASSOCIATED CONTENT

Supporting Information

The Supporting Information is available free of charge on the ACS Publications website at DOI: [10.1021/acs.langmuir.6b03910](https://doi.org/10.1021/acs.langmuir.6b03910).

Validation of Brownian dynamics simulations. Analysis of BD simulations of particle attraction trajectories. Quantification of the drag coefficient in the presence of an attractive capillary interaction. Iterative quantification of f and $F_{0,\text{cap}}$. Contact angle measurement of particles using z-stack images. (PDF)

■ AUTHOR INFORMATION

Corresponding Author

*E-mail: m.w.j.prins@tue.nl.

ORCID

Stefano Cappelli: [0000-0002-4582-2409](https://orcid.org/0000-0002-4582-2409)

Menno W. J. Prins: [0000-0002-9788-7298](https://orcid.org/0000-0002-9788-7298)

Notes

The authors declare no competing financial interest.

■ ACKNOWLEDGMENTS

The research leading to these results has received funding from the European Commission's Seventh Framework Programme (FP7/2007-2013) under grant agreement BIOMAX (project no. 264737).

■ REFERENCES

- (1) Murray, B. S.; Dickinson, E. Interfacial Rheology and the Dynamic Properties of Adsorbed Films of Food Proteins and Surfactants. *Food Sci. Technol. Int., Tokyo* **1996**, *2*, 131–145.
- (2) Rayner, M.; Marku, D.; Eriksson, M.; Sjö, M.; Dejmek, P.; Wahlgren, M. Biomass-based particles for the formulation of Pickering type emulsions in food and topical applications. *Colloids Surf., A* **2014**, *458*, 48–62.
- (3) Lin, Y.; Skaff, H.; Böker, A.; Dinsmore, A. D.; Emrick, T.; Russell, T. P. Ultrathin Cross-Linked Nanoparticle Membranes. *J. Am. Chem. Soc.* **2003**, *125*, 12690–12691.
- (4) Kaufman, G.; Nejati, S.; Sarfati, R.; Boltyanskiy, R.; Loewenberg, M.; Dufresne, E. R.; Osuji, C. O. Soft microcapsules with highly plastic shells formed by interfacial polyelectrolyte-nanoparticle complexation. *Soft Matter* **2015**, *11*, 7478–7482.
- (5) Kinge, S.; Crego-Calama, M.; Reinhoudt, D. N. Self-Assembling Nanoparticles at Surfaces and Interfaces. *ChemPhysChem* **2008**, *9*, 20–42.
- (6) Isa, L.; Kumar, K.; Müller, M.; Grolig, J.; Textor, M.; Reimhult, E. Particle Lithography from Colloidal Self-Assembly at Liquid-Liquid Interfaces. *ACS Nano* **2010**, *4*, 5665–5670.
- (7) Lee, Y. H.; Shi, W.; Lee, H. K.; Jiang, R.; Phang, I. Y.; Cui, Y.; Isa, L.; Yang, Y.; Wang, J.; Li, S.; Ling, X. Y. Nanoscale surface chemistry directs the tunable assembly of silver octahedra into three two-dimensional plasmonic superlattices. *Nat. Commun.* **2015**, *6*, 6990.
- (8) Binks, B. P.; Horozov, T. S. In *Zhurnal Eksperimental'noi i Teoreticheskoi Fiziki*; Binks, B. P., Horozov, T. S., Eds.; Cambridge University Press: New York, 2008; p 520.
- (9) Ershov, D.; Sprakel, J.; Appel, J.; Cohen Stuart, M. A.; van der Gucht, J. Capillarity-induced ordering of spherical colloids on an interface with anisotropic curvature. *Proc. Natl. Acad. Sci. U. S. A.* **2013**, *110*, 9220–9224.
- (10) Barman, S.; Christopher, G. F. Simultaneous Interfacial Rheology and Microstructure Measurement of Densely Aggregated Particle Laden Interfaces Using a Modified Double Wall Ring Interfacial Rheometer. *Langmuir* **2014**, *30*, 9752–9760.
- (11) Mendoza, A. J.; Guzmán, E.; Martínez-Pedrero, F.; Ritacco, H.; Rubio, R. G.; Ortega, F.; Starov, V. M.; Miller, R. Particle laden fluid interfaces: Dynamics and interfacial rheology. *Adv. Colloid Interface Sci.* **2014**, *206*, 303–319.
- (12) Kaufman, G.; Boltyanskiy, R.; Nejati, S.; Thiam, A. R.; Loewenberg, M.; Dufresne, E. R.; Osuji, C. O. Single-step microfluidic fabrication of soft monodisperse polyelectrolyte microcapsules by interfacial complexation. *Lab Chip* **2014**, *14*, 3494.
- (13) Bresme, F.; Oettel, M. Nanoparticles at fluid interfaces. *J. Phys.: Condens. Matter* **2007**, *19*, 413101.
- (14) Oettel, M.; Dietrich, S. Colloidal Interactions at Fluid Interfaces. *Langmuir* **2008**, *24*, 1425–1441.
- (15) Boneva, M. P.; Christov, N. C.; Danov, K. D.; Kralchevsky, P. A. Effect of electric-field-induced capillary attraction on the motion of particles at an oil-water interface. *Phys. Chem. Chem. Phys.* **2007**, *9*, 6371.
- (16) Stamou, D.; Duschl, C.; Johannsmann, D. Long-range attraction between colloidal spheres at the air-water interface: The consequence of an irregular meniscus. *Phys. Rev. E: Stat. Phys., Plasmas, Fluids, Relat. Interdiscip. Top.* **2000**, *62*, 5263–5272.
- (17) Kralchevsky, P. A.; Nagayama, K. Capillary interactions between particles bound to interfaces, liquid films and biomembranes. *Adv. Colloid Interface Sci.* **2000**, *85*, 145–192.
- (18) Park, B. J.; Lee, D.; Furst, E. M. *Particle-Stabilized Emulsions and Colloids: Formation and Applications*; Ngai, T., Bon, S. A. F., Eds.; Royal Society of Chemistry: Cambridge, 2015; Chapter 2, pp 8–44.
- (19) Loudet, J. C.; Alsayed, A. M.; Zhang, J.; Yodh, A. G. Capillary Interactions Between Anisotropic Colloidal Particles. *Phys. Rev. Lett.* **2005**, *94*, 018301.
- (20) Danov, K. D.; Kralchevsky, P. A. Capillary forces between particles at a liquid interface: general theoretical approach and interactions between capillary multipoles. *Adv. Colloid Interface Sci.* **2010**, *154*, 91–103.
- (21) Botto, L.; Lewandowski, E. P.; Cavallaro, M.; Stebe, K. J. Capillary interactions between anisotropic particles. *Soft Matter* **2012**, *8*, 9957.
- (22) Davies, G. B.; Krüger, T.; Coveney, P. V.; Harting, J.; Bresme, F. Interface deformations affect the orientation transition of magnetic ellipsoidal particles adsorbed at fluid-fluid interfaces. *Soft Matter* **2014**, *10*, 6742–8.
- (23) Zwanzig, R.; Mountain, R. D. High-Frequency Elastic Moduli of Simple Fluids. *J. Chem. Phys.* **1965**, *43*, 4464.
- (24) Masschaele, K.; Park, B. J.; Furst, E. M.; Franssaer, J.; Vermant, J. Finite Ion-Size Effects Dominate the Interaction between Charged Colloidal Particles at an Oil-Water Interface. *Phys. Rev. Lett.* **2010**, *105*, 048303.

- (25) Madivala, B.; Fransaer, J.; Vermant, J. Self-assembly and rheology of ellipsoidal particles at interfaces. *Langmuir* **2009**, *25*, 2718–28.
- (26) Cavallaro, M.; Botto, L.; Lewandowski, E. P.; Wang, M.; Stebe, K. J. Curvature-driven capillary migration and assembly of rod-like particles. *Proc. Natl. Acad. Sci. U. S. A.* **2011**, *108*, 20923–8.
- (27) Aveyard, R.; Binks, B. P.; Clint, J. H.; Fletcher, P. D. I.; Horozov, T. S.; Neumann, B.; Paunov, V. N.; Annesley, J.; Botchway, S. W.; Nees, D.; Parker, A. W.; Ward, A. D.; Burgess, A. N. Measurement of Long-Range Repulsive Forces between Charged Particles at an Oil-Water Interface. *Phys. Rev. Lett.* **2002**, *88*, 246102.
- (28) Neuman, K. C.; Nagy, A. Single-molecule force spectroscopy: optical tweezers, magnetic tweezers and atomic force microscopy. *Nat. Methods* **2008**, *5*, 491–505.
- (29) Park, B. J.; Furst, E. M. Attractive interactions between colloids at the oil-water interface. *Soft Matter* **2011**, *7*, 7676.
- (30) Maestro, A.; Guzmán, E.; Ortega, F.; Rubio, R. G. Contact angle of micro- and nanoparticles at fluid interfaces. *Curr. Opin. Colloid Interface Sci.* **2014**, *19*, 355–367.
- (31) Maestro, A.; Bonales, L. J.; Ritacco, H.; Fischer, T. M.; Rubio, R. G.; Ortega, F. Surface rheology: macro- and microrheology of poly(tert-butyl acrylate) monolayers. *Soft Matter* **2011**, *7*, 7761.
- (32) Samaniuk, J. R.; Vermant, J. Micro and macrorheology at fluid-fluid interfaces. *Soft Matter* **2014**, *10*, 7023–7033.
- (33) Dhar, P.; Cao, Y.; Fischer, T. M.; Zasadzinski, J. A. Active Interfacial Shear Microrheology of Aging Protein Films. *Phys. Rev. Lett.* **2010**, *104*, 016001.
- (34) Allan, D. B.; Firester, D. M.; Allard, V. P.; Reich, D. H.; Stebe, K. J.; Leheny, R. L. Linear and nonlinear microrheology of lysozyme layers forming at the air-water interface. *Soft Matter* **2014**, *10*, 7051–7060.
- (35) Choi, S.; Steltenkamp, S.; Zasadzinski, J.; Squires, T. Active microrheology and simultaneous visualization of sheared phospholipid monolayers. *Nat. Commun.* **2011**, *2*, 312.
- (36) Reynaert, S.; Moldenaers, P.; Vermant, J. Control over Colloidal Aggregation in Monolayers of Latex Particles at the Oil-Water Interface. *Langmuir* **2006**, *22*, 4936–4945.
- (37) Park, B. J.; Pantina, J. P.; Furst, E. M.; Oettel, M.; Reynaert, S.; Vermant, J. Direct Measurements of the Effects of Salt and Surfactant on Interaction Forces between Colloidal Particles at Water-Oil Interfaces. *Langmuir* **2008**, *24*, 1686–1694.
- (38) van Reenen, A.; Gao, Y.; Bos, A. H.; de Jong, A. M.; Hulslen, M. A.; den Toonder, J. M. J.; Prins, M. W. J. Accurate quantification of magnetic particle properties by intra-pair magnetophoresis for nanobiotechnology. *Appl. Phys. Lett.* **2013**, *103*, 043704.
- (39) Cappelli, S.; de Jong, A. M.; Baudry, J.; Prins, M. W. J. Interfacial rheometry of polymer at a water-oil interface by intra-pair magnetophoresis. *Soft Matter* **2016**, *12*, 5551–5562.
- (40) Danov, K. D.; Kralchevsky, P. A.; Naydenov, B. N.; Brenn, G. Interactions between particles with an undulated contact line at a fluid interface: Capillary multipoles of arbitrary order. *J. Colloid Interface Sci.* **2005**, *287*, 121–134.
- (41) Xie, Q.; Davies, G. B.; Günther, F.; Harting, J. Tunable dipolar capillary deformations for magnetic Janus particles at fluid-fluid interfaces. *Soft Matter* **2015**, *11*, 3581–3588.
- (42) Hurd, A. J. The electrostatic interaction between interfacial colloidal particles. *J. Phys. A: Math. Gen.* **1985**, *18*, L1055–L1060.
- (43) Danov, K.; Aust, R.; Durst, F.; Lange, U. Influence of the Surface Viscosity on the Hydrodynamic Resistance and Surface Diffusivity of a Large Brownian Particle. *J. Colloid Interface Sci.* **1995**, *175*, 36–45.
- (44) Fischer, T. M.; Dhar, P.; Heinig, P. The viscous drag of spheres and filaments moving in membranes or monolayers. *J. Fluid Mech.* **2006**, *558*, 451.
- (45) Squires, T. M.; Mason, T. G. Fluid Mechanics of Microrheology. *Annu. Rev. Fluid Mech.* **2010**, *42*, 413–438.
- (46) Zell, Z. A.; Nowbahar, A.; Mansard, V.; Leal, L. G.; Deshmukh, S. S.; Mecca, J. M.; Tucker, C. J.; Squires, T. M. Surface shear inviscidity of soluble surfactants. *Proc. Natl. Acad. Sci. U. S. A.* **2014**, *111*, 3677–3682.
- (47) Borkovec, M.; Szilagy, I.; Popa, I.; Finessi, M.; Sinha, P.; Maroni, P.; Papastavrou, G. Investigating forces between charged particles in the presence of oppositely charged polyelectrolytes with the multi-particle colloidal probe technique. *Adv. Colloid Interface Sci.* **2012**, *179–182*, 85–98.
- (48) Grassia, P. S.; Hinch, E. J.; Nitsche, L. C. Computer simulations of Brownian motion of complex systems. *J. Fluid Mech.* **1995**, *282*, 373.
- (49) Dünweg, B.; Paul, W. Brownian dynamics simulations without Gaussian random numbers. *International Journal of Modern Physics C* **1991**, *02*, 817–827.
- (50) Ermak, D. L.; McCammon, J. A. Brownian dynamics with hydrodynamic interactions. *J. Chem. Phys.* **1978**, *69*, 1352.
- (51) Northrup, S. H.; Allison, S. A.; McCammon, J. A. Brownian dynamics simulation of diffusion-influenced bimolecular reactions. *J. Chem. Phys.* **1984**, *80*, 1517.
- (52) Noskov, B. A. Dilational surface rheology of polymer and polymer/surfactant solutions. *Curr. Opin. Colloid Interface Sci.* **2010**, *15*, 229–236.
- (53) Brenner, H. The slow motion of a sphere through a viscous fluid towards a plane surface. *Chem. Eng. Sci.* **1961**, *16*, 242–251.
- (54) Rezvantlab, H.; Shojaei-Zadeh, S. Capillary interactions between spherical Janus particles at liquid-fluid interfaces. *Soft Matter* **2013**, *9*, 3640.
- (55) Davies, G. B.; Krüger, T.; Coveney, P. V.; Harting, J.; Bresme, F. Interface deformations affect the orientation transition of magnetic ellipsoidal particles adsorbed at fluid-fluid interfaces. *Soft Matter* **2014**, *10*, 6742.
- (56) Ward, A. F. H.; Tordai, L. Time-Dependence of Boundary Tensions of Solutions I. The Role of Diffusion in Time-Effects. *J. Chem. Phys.* **1946**, *14*, 453.
- (57) Eastoe, J.; Dalton, J. Dynamic surface tension and adsorption mechanisms of surfactants at the air-water interface. *Adv. Colloid Interface Sci.* **2000**, *85*, 103–144.
- (58) Kaz, D. M.; McGorty, R.; Mani, M.; Brenner, M. P.; Manoharan, V. N. Physical ageing of the contact line on colloidal particles at liquid interfaces. *Nat. Mater.* **2012**, *11*, 138–142.
- (59) Chen, L.; Heim, L.-O.; Golovko, D. S.; Bonaccorso, E. Snap-in dynamics of single particles to water drops. *Appl. Phys. Lett.* **2012**, *101*, 031601.
- (60) Cappelli, S.; Xie, Q.; Harting, J.; de Jong, A. M.; Prins, M. W. J. Dynamic wetting: status and prospective of single particle based experiments and simulations. *New Biotechnol.* **2015**, *32*, 420–432.
- (61) van Heiningen, J. A.; Hill, R. J. Poly(ethylene oxide) Adsorption onto and Desorption from Silica Microspheres: New Insights from Optical Tweezers Electrophoresis. *Macromolecules* **2011**, *44*, 8245–8260.
- (62) Maestro, A.; Hilles, H. M.; Ortega, F.; Rubio, R. G.; Langevin, D.; Monroy, F. Reptation in langmuir polymer monolayers. *Soft Matter* **2010**, *6*, 4407.
- (63) van Reenen, A.; Gutiérrez-Mejía, F.; van Ijzendoorn, L. J.; Prins, M. W. J. Torsion Profiling of Proteins Using Magnetic Particles. *Biophys. J.* **2013**, *104*, 1073–1080.
- (64) Günther, F.; Janoschek, F.; Frijters, S.; Harting, J. Lattice Boltzmann simulations of anisotropic particles at liquid interfaces. *Comput. Fluids* **2013**, *80*, 184–189.